JOURNAL OF AIRCRAFT
Vol. 43, No. 3, May–June 2006

Oscillating-Wing Tip Vortex with Passive Short-Span Trailing-Edge Flaps

L. Lee* and T. Lee†
McGill University, Montreal, Quebec H3A 2K6, Canada

Tip vortex flow behind an oscillating NACA 0015 wing with passive short-span trailing-edge flaps was investigated experimentally at $Re = 1.81 \times 10^5$. The spoiler was found to be very effective in diffusing the tip vortex, in terms of the reduction of peak tangential velocity $v_{\theta\text{peak}}$ and vortex strength, compared to a baseline wing, and also led to additional vertical upward displacement of the vortex center. No significant influence on the vortex size was observed, however. The spoiler-induced negative camber effects also translated into slightly reduced bound circulation, total lift, and lift-induced drag. For a tab, the dynamic increase–decrease in the vortex size and strength persisted and had values larger than for a baseline wing. No substantial change in $v_{\theta\text{peak}}$, compared to that for a baseline wing, was noticed. The axial core velocity was always wakelike, and the vortex center was shifted relatively outboard and vertically downward below the baseline wing. The tab also led to an increase in the lift and drag forces. The symmetric flap provided a compromise in the critical vortex-flow quantities between the spoiler and tab cases.

Nomenclature

b	=	(semi-)wing span
C_D	=	total drag coefficient
C_{Di}	=	induced drag coefficient, $= D_i/\frac{1}{2}\rho u_\infty^2 S$
C_L	=	total lift coefficient, $= L/\frac{1}{2}\rho u_\infty^2 S$
c	=	airfoil chord
D_i	=	induced drag
f	=	oscillation frequency
L	=	total lift
Re	=	Reynolds number, $= cu_\infty/\nu$
r_c	=	vortex core radius
r_o	=	vortex outer radius
S	=	wing area
t	=	time
u	=	mean axial velocity
u_∞	=	freestream velocity
u'	=	axial turbulence, $(u'^2)^{\frac{1}{2}}$
v	=	transverse mean velocity
v_θ	=	tangential velocity
w	=	spanwise mean velocity
x	=	streamwise distance
y	=	transverse distance
α	=	angle of attack
Γ	=	circulation or vortex strength
Γ_b	=	bound or root circulation
Γ_c	=	core circulation
Γ_o	=	total circulation
κ	=	reduced frequency, $= \pi fc/u_\infty$
ζ	=	streamwise or axial vorticity
ν	=	kinematic viscosity
ρ	=	fluid density

Subscripts

d	=	pitch-down
u	=	pitch-up

Received 8 April 2005; revision received 2 August 2005; accepted for publication 2 August 2005.

*Research Assistant.
†Associate Professor, Department of Mechanical Engineering. Member AIAA.

I. Introduction

COUNTER-ROTATING longitudinal vortices generated by aircraft wing tips, because of their hazardous effects on flight safety and airport capacity, continue to be of concern to the aviation industry and aircraft manufacturers alike. Near-field tip vortex flow also plays a significant role in the understanding and control of rotorcraft blade–vortex interaction (BVI) noise and vibration. However, in contrast to a fixed wing, which has relatively uniform lift loading over its span, a concentration of aerodynamic forces is produced at helicopter blade tips, due to the high local dynamic pressure, which, consequently, shed strong vortices at each blade tip. Moreover, during low-speed forward flight, the strength and position of the shed tip vortex may also be significantly affected by the retreating-blade dynamic-stall flow phenomenon.

It is now well known that the predominant feature of dynamic stall is the formation, convection, and shedding over the upper surface of the airfoil of an energetic leading-edge vortex (LEV), or a dynamic stall vortex, which induces a nonlinearly fluctuating pressure field and produces large transient variations in forces and moments that are fundamentally different from their static counterparts. The presence of a LEV leads to delayed stall through the delay of large separation effects to increased angles of attack and enables the rapid generation of significant unsteady lift forces before any vorticity is shed. After the LEV begins convecting over the airfoil there is a sudden increase in nose-down pitching moment, and once the LEV passes the airfoil trailing edge and moves into the wake, the flow progresses to a state of full separation over the upper surface and an abrupt loss of lift is incurred. Furthermore, if and when the angle of attack becomes low enough during the pitch-down motion, the flow will finally reattach again from the leading edge. An excellent review of unsteady airfoils is given by McCroskey.[1] However, unlike the considerable experimental and numerical efforts made toward the understanding and control of the tip vortex generated by a fixed-wing tip, only limited results have been reported, to the authors' knowledge, on the tip vortex generated behind an oscillating wing.[2–4]

Ramaprian and Zheng[3] pioneered the quantitative study of the near field of the tip vortex behind a square-tipped oscillating NACA 0015 rectangular wing using a three-component laser Doppler anemometer at $Re = 1.8 \times 10^5$ with $\alpha(t) = 10^\circ + 5^\circ \sin \omega t$ (i.e., the light-stall oscillation case[1,5]) and a reduced frequency κ of 0.1. They explored the unsteady velocity and vorticity fields associated with the evolving tip vortex in the near field for $0.16 < x/c < 2.66$ and observed that the average trajectory of the oscillating tip vortex was very nearly the same as for a stationary wing at the mean

incidence. Also, the normalized circulation distribution across most of the inner region of the vortex for $x/c > 0.7$ exhibited the same universal behavior as the vortex behind a stationary wing. Chang and Park[4] examined the hysteretic behavior of the wake behind a NACA 0012 airfoil oscillated with $\alpha(t) = 15^\circ + 15^\circ \sin \omega t$ (i.e., the deep-stall oscillation case[1,5]) at $\kappa = 0.09$ for $Re = 3.4 \times 10^4$ using a triple hot-film probe at $x/c = 0.5$ and 1.5. Chang and Park found that the size of the vortex core and the vortex strength were larger and the peak tangential velocity and the axial velocity deficit were smaller during pitch-down than during pitch-up. The details of the vortex-flow characteristics, however, were not reported in the Technical Note.

On the other hand, the interactions of concentrated tip vortices with rotor blades are known to have an adverse influence on rotor aerodynamics. When these shed vortices interact with the trailing rotor blades, the unsteady pressure fluctuations induced on the blade surfaces generally lead to severe dynamic structural loading and noise generation. The blade–vortex interaction and BVI noise is most likely to occur during helicopter low-speed forward flight and descent. The interaction process is shown to involve a combination of effects on the vortex structure, the strength, and the miss distance between a vortex and a blade. Various control devices,[6–13] such as passive Ogee tips, winglets, spoilers, stub/subwings, and porous tips and leading edges, as well as active higher harmonic control, individual blade control, trailing-edge flaps, and steady and pulsating injection, have been attempted to modify the vortex strength and structure and the miss distance at the time of vortex production and interaction. Among them, short-span spoilers located at the trailing edge of the airfoil on the pressure side and perpendicular to the chord, similar to a full-span Gurney flap,[14] were found to be very effective in diffusing the tip vortex by Liu et al. computationally.[7] However, detailed documentation of the vortex-flow quantities is still needed.

The objective of this study was to investigate the near-field tip vortex- flow structure behind an oscillating NACA 0015 airfoil with and without short-span trailing-edge flaps at $Re = 1.81 \times 10^5$ using a miniature triple hot-wire probe. Three different flap configurations, of a 2.3%c hight (scaled with the boundary-layer thickness at the wing trailing edge), including a symmetric arrangement, were tested. The outboard edge of the spoiler and the tab were aligned with the wing tip and were fitted normal to the local curvature on the lower and/or upper surface at the trailing edge of the wing model. Particular attention was given to the behavior of the phase-locked ensemble-averaged crossflow and axial velocity fields, the vorticity distribution, the turbulence structure, and the strength, size, and trajectory of the vortex over one cycle of oscillation. Furthermore, by means of thin-airfoil theory, the contributions to the total lift and lift-induced drag from the short-span flaps were also estimated.

II. Experimental Methods

The experiment was conducted in the new $0.9 \times 1.2 \times 2.7$ m low-speed, suction-type wind tunnel at McGill University with a freestream turbulence intensity of 0.03% at $u_\infty = 35$ m/s. A square-tipped, untwisted, and rectangular NACA 0015 airfoil, fabricated from solid aluminum, with a chord length c of 20.3 cm and a (semi)span b of 49.5 cm, was used as the test model. The wing model was mounted horizontally at the center of the wind-tunnel test section. A 40-cm-diam aluminum endplate with sharp leading edges was fixed to an end support located 20 cm from the sidewall of the test section. The gap between the wing and the endplate was kept at less than 1 mm to minimize the leakage flow through the gap. The origin of the coordinates was located at the trailing edge of the airfoil with x, y, and z in the streamwise, normal, and spanwise directions, respectively. The two-dimensional uniformity of the flow distribution over the airfoil model (with the addition of a second endplate to the tip of the wing) was checked by traversing a 5-μm normal hot-wire probe located 30%c downstream from the leading edge of the airfoil and $y = 5$ mm above the airfoil. The nonuniformity was found to be $\pm 3\%$ of the freestream value. The freestream velocity was fixed at 14.2 m/s, which rendered a chord Reynolds number of 1.81×10^5.

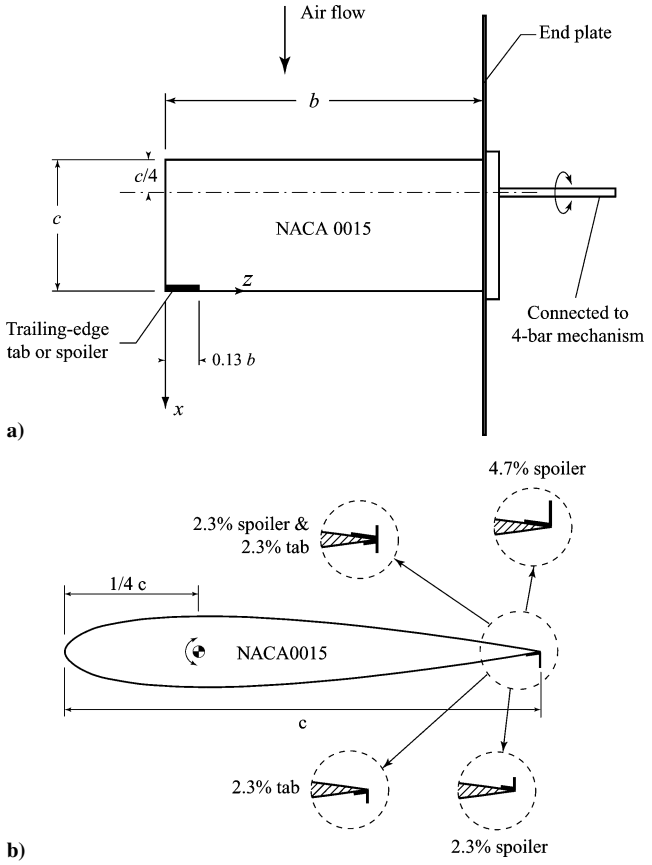

Fig. 1 a) Oscillating wing mechanism and b) short-span trailing-edge flap configuration.

The effect of the short-span trailing-edge flap size was investigated by testing a flap height h of 2.3% chord with thickness of 0.15% chord and a width of 13% span. The flap was located at the trailing edge, centered at 93.5% span position, and was fitted normal to the local curvature, on the lower (referred to as the tab) or upper (referred to as the spoiler) surface, at the trailing edge of the wing model. A symmetric flap formed by a combination of a 2.3%c spoiler and a 2.3%c tab was also tested. The short-span flaps were attached to the trailing edge using double-sided Mylar adhesive film. The flap dimensions and configurations are given in Fig. 1. A specially designed four-bar linkage and flywheel oscillation mechanism, capable of oscillating the airfoil sinusoidally at various amplitudes and frequencies, mounted on the exterior of the wind tunnel, was used in the present experiment. The mean angle of attack was varied by changing the relative angle between the rotating shaft and the rocker–shaft connector. The oscillation amplitude was varied by attaching the coupler at specific radial locations on the flywheel. The flywheel was attached directly to an Exlar Model DXM34C servomotor driven by an Emerson Model FX316/PCM1 programmable motion controller. The oscillation frequency was measured to an accuracy of ± 0.02 Hz. The four-bar mechanism provided an output that was sinusoidal to within 2%. The airfoil pitch axis was located at $\frac{1}{4}$-chord location. The instantaneous angle of attack $\alpha(t) (= 14^\circ + 8^\circ \sin \omega t$, where $\omega = 2\pi f$ is the circular frequency) of the airfoil and the phase reference signal $\tau = \omega t$ were recorded from both the servomotor feedback resolver and a potentiometer mounted on the servomotor shaft. The airfoil was oscillated through the static-stall angle $\alpha_{ss} = 16.5^\circ$ with a reduced frequency κ of 0.093. A representative dynamic-lift coefficient loop of a two-dimensional NACA 0015 oscillating wing with no tip effects, obtained from the integration of the surface pressure distribution, is shown in Fig. 2, which clearly manifests the various dynamic-stall events, as mentioned previously in Section I, compared to a static wing. The surface-pressure distributions were obtained from a second NACA 0015 wing model equipped with

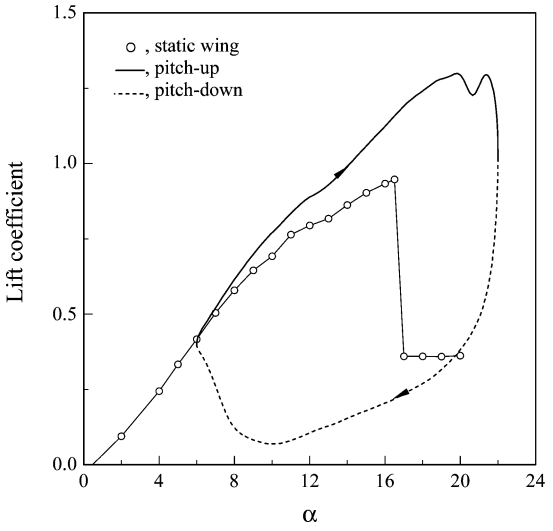

Fig. 2 Lift coefficient curves of a two-dimensional NACA 0015 wing.

48 pressure orifices covering $x/c = 0$ to 96.5%. Also, in the following discussion, the suffix u is used to indicate pitch-up when α is increasing and d is used to indicate pitch-down when α is decreasing.

The instantaneous velocities were subsequently ensemble-averaged over 40–80 oscillating cycles to obtain phased-locked averages of the flow properties at various phase positions during the cycle. A miniature triple hot-wire probe (Auspex Model AVEP-3-102 with measurement volume 0.5 mm^3) was used to measure the mean and fluctuating velocity components. The mean flowfields behind the static wing was also examined using a seven-hole pressure probe (with outside diameter 2.4 mm), which was used to validate the corresponding triple hot-wire mean velocity measurements. The pressure probe and triple hot-wire probe were calibrated in situ, following the calibration procedures described by Wenger and Devenport[15] and Chow et al.,[16] respectively, before the installation of the model. The low-pass filtered pressure and hot-wire signals were sampled at 500 Hz and were recorded on a personal computer through a 16-bit A/D converter board. Probe traversing was achieved through a custom-built computer-controlled traversing system with position resolution of 20 μm in all three directions. The three-dimensional velocities downstream of the trailing edge of the wing were measured in planes perpendicular to the freestream velocity at $x/c = 2.0$. Data planes taken in the near field of the wing models had 46×92 measuring grid points with an increment of $\Delta y = \Delta z = 3.2$ mm. Note that due to the limitation of the probe traversing mechanism, the present wake survey region did not encompass the entire wake: only 87% of the wing wake was measured.

The maximum experimental uncertainties in the results reported have been estimated as follows[17]: mean velocity 3.5%, vorticity component 8%, vortex radius 4%, and velocity fluctuation 3%. No wind-tunnel wall corrections were made to the present measurements. Furthermore, it is known that the lateral excursions to which a trailing vortex is prone when situated in a freestream containing ambient turbulence have long cause problems in measurement of vortex characteristics, and that the meander amplitude increases with the level of freestream turbulence and with the downstream distance from the generating lifting surface. However, the vortex meandering in the near field behind the static generating wing was examined in the present low-turbulence wind tunnel using the correlation technique/criteria employed by Chow et al.[16] The meandering of the vortex was found to be small in the present experiment.

III. Results and Discussion

To facilitate the investigation of the effects of the short-span trailing-edge flaps on the nondimensional phase-locked ensemble-averaged tip vortex-flow quantities behind a NACA 0015 wing oscillated with $\alpha(t) = 14^\circ + 8^\circ \sin \omega t$ and $\kappa = 0.093$, the tip vortex behind an oscillating baseline wing at $x/c = 2.0$ was characterized first and serves as a reference.

A. Baseline Wing

The dynamic loops of the critical vortex flow quantities and the vortex trajectory of an oscillating baseline wing are presented in Figs. 3a–3e. Also shown in Fig. 3 are the static-wing data. Figure 3a shows that for a baseline wing, the peak tangential velocity $v_{\theta\text{peak}}$ increased with α and was found to be considerably lower during pitch-down than during pitch-up (due to the LEV-induced massive flow separation). The dynamic value of $v_{\theta\text{peak}}$ was always below that of a static wing for $\alpha \le \alpha_{ss}$, whereas it continued to increase above the static-wing value for $\alpha_{ss} < \alpha < \alpha_{max}$ during pitch-up, attributed to the boundary-layer improvement and LEV transient effects.[18] A similar increase–decrease trend in the magnitude of core vorticity during pitch-up and pitch-down (not shown here) was also exhibited. Figure 3a also shows that for a static wing, the axial core velocity u_c of the tip vortex was wakelike for $\alpha < 10^\circ$ and became jetlike for $10^\circ < \alpha < 18^\circ$. The axial core velocity was, however, found to be persistently wakelike and was decreased with increasing α during pitch-up. During pitch-up, the variation of u_c was characterized by a sharp rise and drop at $\alpha_d = 19^\circ$ (with a local peak u_c of $1.3u_\infty$, compared to $0.63u_\infty$ at $\alpha_u = 21^\circ$) and then remained virtually unchanged with $u_c \approx u_\infty$ for $\alpha_d < \alpha_{ss}$, except in the vicinity of α_{min}. Moreover, in contrast to the considerably higher value observed in $v_{\theta\text{peak}}$ during pitch-up than during pitch-down, the u_c had a much lower value during pitch-up than during pitch-down.

The variation of the vortex core radius r_c (defined as the radius at which v_θ is a maximum) and outer radius r_o (obtained by measuring the extent as $\Gamma(r_o)$ reached 98% of the total circulation) with α of both a static wing and an oscillating baseline wing are displayed in Fig. 3b. The vortex center was taken as the position of local maximum vorticity. For an oscillating wing, the vortex size not only increased (above the static-wing value) with increasing α, but also had larger values during pitch-down than during pitch-up. The dynamic loops of the nondimensional total Γ_o and core Γ_c circulation of the tip vortex are presented in Fig. 3c. The circulation was computed based on Stokes's theorem. The increase–decrease trend observed in Γ during pitch-up and pitch-down was found to be similar to the dynamic behavior of the lift coefficient curve shown in Fig. 2. It is, however, noteworthy that because of the convection time required for a tip vortex-flow structure to propagate from the wing to the downstream location of the sensor, there is a phase lag between any instantaneous sensor reading and the position of the wing at that instant. By assuming that within the streamwise length-scale considered, any streamwise distortion of the flow structure that occurs is negligible, and that the convection speed u_{conv} is constant, thus the angle of attack through which the wing has swept during the convection time can be directly calculated. An upper and lower bound are generally imposed upon the convection speed, because it cannot fall outside of the range of axial velocities measured within the volume through which it has moved. In the present experiment, u_{conv} was approximated as the upper-bound freestream speed, because it resulted in the smallest phase-lag correction, a phase-lag compensation scheme suggested by Chang and Park.[4] The compensated and uncompensated dynamic Γ_o loops and the angles of attack are presented in Fig. 3d and Table 1, respectively. The measurements reported in this study were phase-lag compensated by letting $u_{conv} = u_\infty$.

Figure 3c also clearly demonstrates the hysteretic property existing in the dynamic Γ_o and Γ_c loops between pitch-up and pitch-down. For an oscillating wing, both the values of Γ_c and Γ_o increased with increasing α and had higher circulation during pitch-up than during pitch-down. Furthermore, for $\alpha_u \le \alpha_{ss}$, there was a slight increase in the vortex strength, compared to their static counterparts (due to the boundary-layer improvement effects[18]), suggesting a less turbulent and better organized tip vortex with a slightly stronger circulation during the pitch-up attached-flow regime. For $\alpha_{ss} < \alpha_u < \alpha_{max}$, the values of Γ_c and Γ_o continued to increase, as

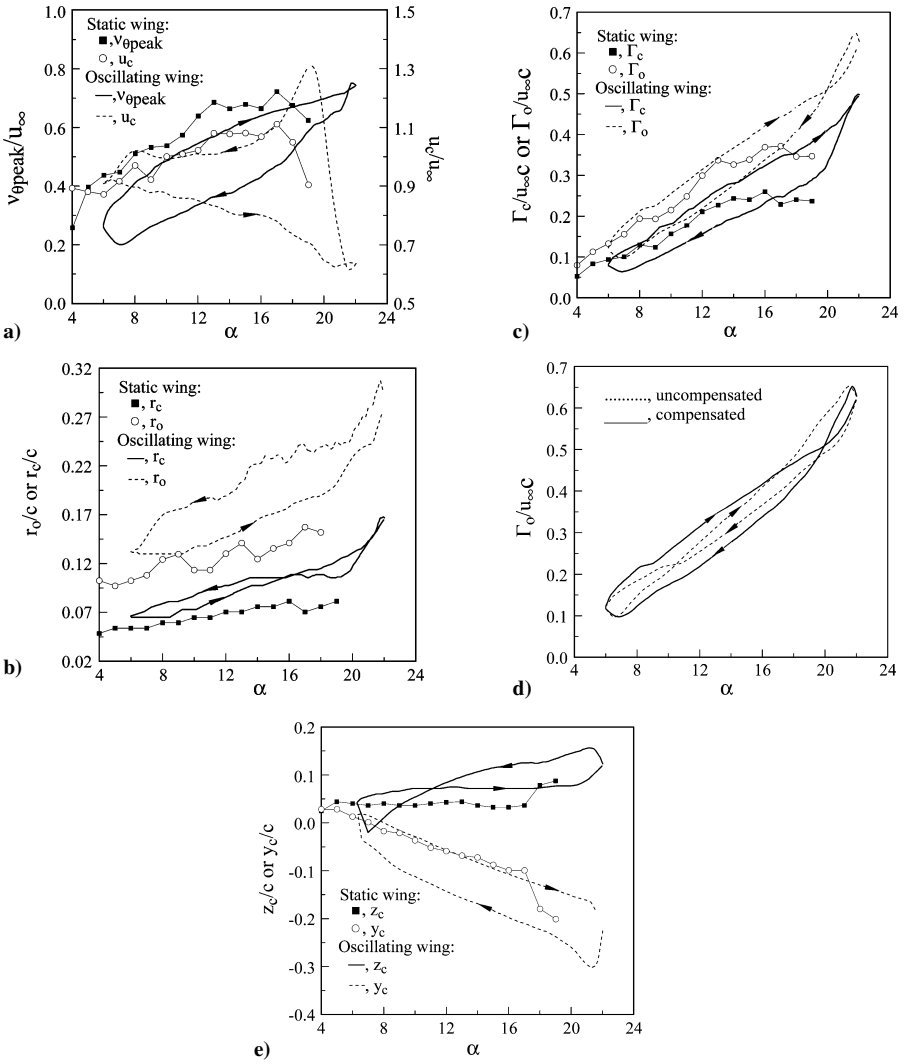

Fig. 3 Baseline-wing critical vortex flow quantities.

Table 1 Compensated and uncompensated angles of attack in degrees

Pitch-up		Pitch-down	
Uncompensated	Compensated	Uncompensated	Compensated
6	6	22	22.21
7	6.59	21	21.62
8	7.19	20	21.00
9	7.82	19	20.35
10	8.49	18	19.65
11	9.22	17	18.89
12	10.01	16	18.07
13	10.87	15	17.17
14	11.81	14	16.19
15	12.83	13	15.13
16	13.93	12	13.99
17	15.10	11	12.78
18	16.35	10	11.51
19	17.65	9	10.18
20	18.99	8	8.81
21	20.38	7	7.41
22	21.79	6	6

a result of the presence of flow reversal and the LEV transient effects, and were found to be significantly higher than the static-wing values. During pitch-down with $\alpha_d \leq \alpha_{ss}$, the vortex strength was, however, found to be lower than for a static wing. Moreover, the position of the vortex center during one oscillation cycle was found to be shifted further inboard and vertically downward below the wing, especially, during the pitch-down motion, compared to that for a static wing (Fig. 3e).

B. Wing with a Spoiler

The effect of short-span trailing-edge flaps on the variation of the vortex-flow structure, specifically $v_{\theta\text{peak}}$, vortex size and strength, and vortex trajectory, compared to a baseline wing, is summarized in Figs. 4–7. The results show that with the addition of a spoiler of height 2.3%c, the changes in vortex structure can best be emphasized by the measurement of the isovorticity contours (Fig. 4b) and the strength of the tip vortex (Fig. 5). For clarity, only the tip vortex is shown in Fig. 4, although as much as 87% of the wake was measured. It is evident that the presence of a spoiler promoted trailing-edge flow separation and shifted the lift curve vertically downward (similarly to an inverted Gurney flap[14]) during pitch-up, and, consequently, caused, a reduction in the vorticity contour levels (Fig. 4b), compared to those for a baseline wing (Fig. 4a). As a result of the spoiler-induced negative effective camber effects, especially in the trailing-edge region, there was a drastic reduction in vortex strength, especially in Γ_c, during pitch-up, compared to that for a baseline wing (Figs. 5a and 5b); a minor reduction in the vortex strength was, however, observed during pitch-down due to the fact that the spoiler was completely embedded in a largely separated flow. The hysteresis loop of Γ_c was greatly reduced, which was attributed to the negative effective camber effects-induced substantial lift reduction during pitch-up and the largely unaffected lift performance during pitch-down. It is of significance to note that the substantial reduction in Γ_c during pitch-up (Fig. 5a), compared to that for a baseline wing, further suggests that the spoiler-equipped wing was very effective in the alleviation of the strength of a tip vortex. A direct comparison of typical vortex-flow distributions across the vortex center of the spoiler-equipped wing with those of a baseline wing is presented

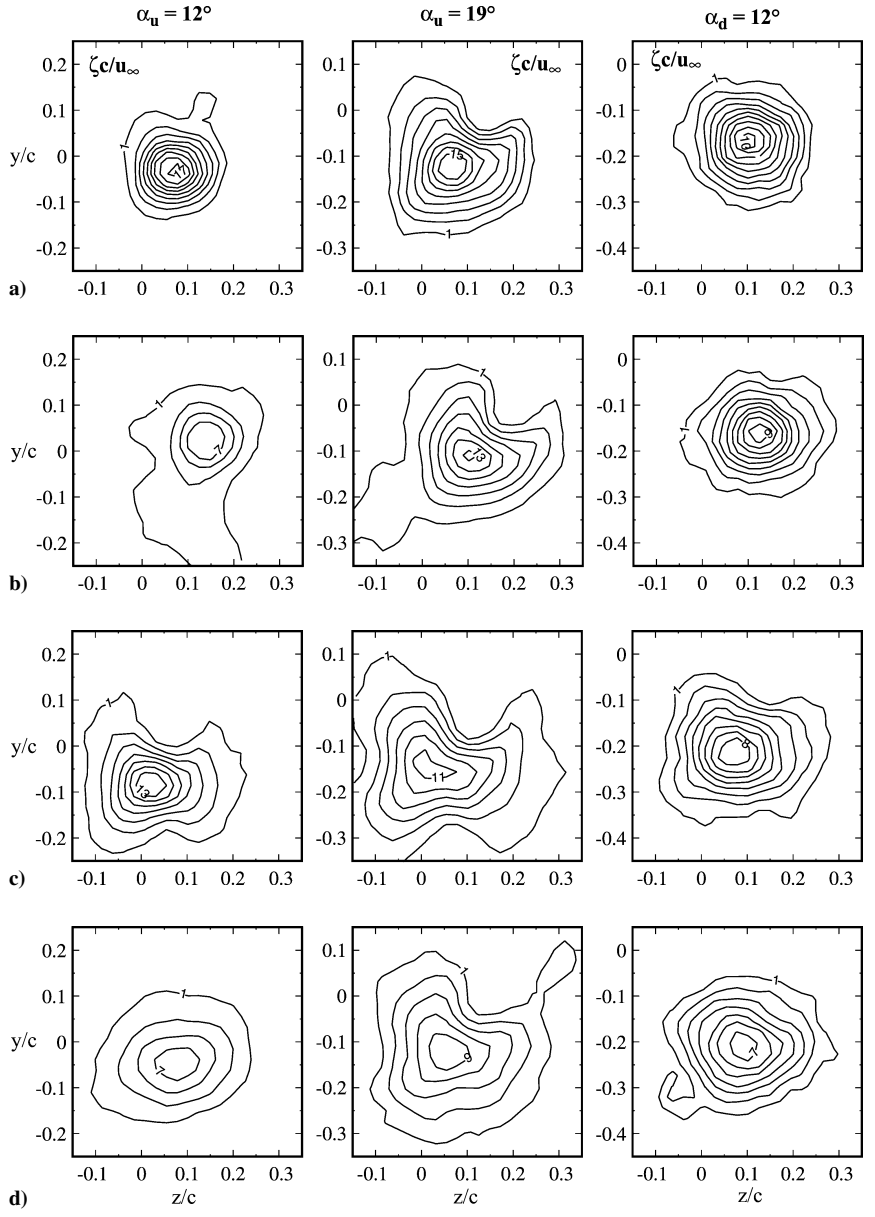

Fig. 4 Normalized isovorticity contour with an increment of 2: a) baseline wing, b) (2.3%)*c* spoiler, c) (2.3%)*c* tab, and d) symmetric configuration.

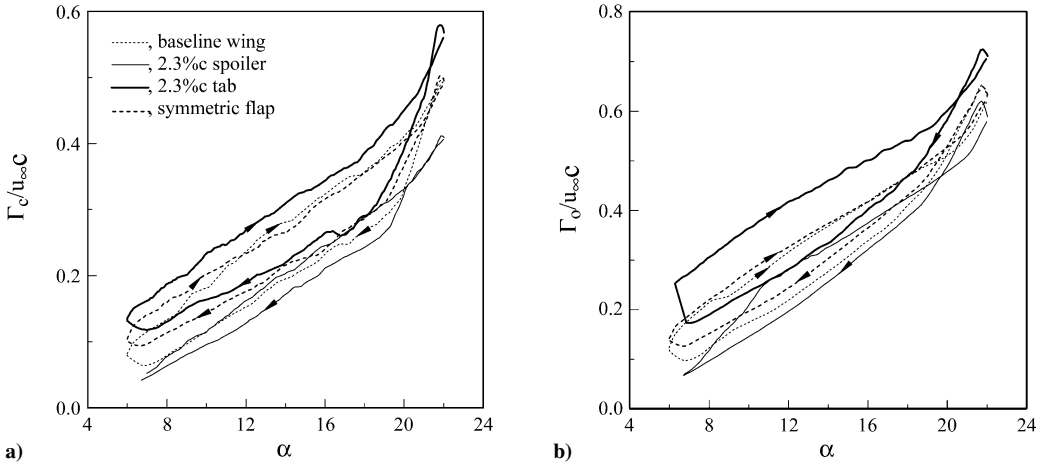

Fig. 5 Dynamic loops of core and total circulation.

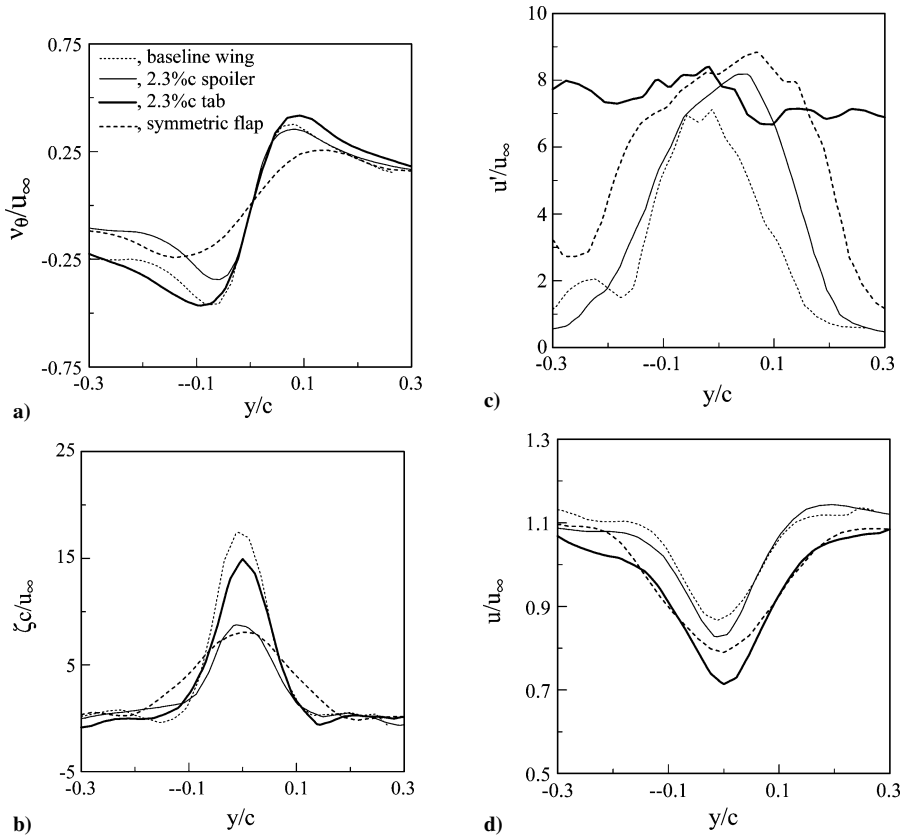

Fig. 6 Typical vortex flow distribution across the vortex center for $\alpha_u = 12°$.

in Fig. 6 for $\alpha_u = 12°$. Figure 6 clearly indicates that the spoiler caused rapid radial redistribution of rotational velocity and vorticity, as a result of the higher level of turbulence (Fig. 6c) induced by an earlier boundary-layer flow separation, compared to that of a baseline wing, for $\alpha_u < \alpha_{ss}$. The reduction in ζ and v_θ (Figs. 6a and 6b) and the increase in u' also led to increased axial wake deficit (Fig. 6d).

The effect of a spoiler on the dynamic curves of the critical vortex-flow quantities (i.e., $v_{\theta\text{peak}}$, u_c, r_c, and r_o) and the vortex trajectory over one oscillation cycle are summarized in Figs. 7a–7f. Figure 7a further demonstrates that the most noticeable quality, in addition to the reduction in the vortex strength, was the lack of high rotational/tangential velocities in the center region of the tip vortex, due to the unloading of the tip region by the use of a spoiler. Similarly to the case of a baseline wing, $v_{\theta\text{peak}}$ had higher values during pitch-up than during pitch-down. A substantial reduction in $v_{\theta\text{peak}}$ during pitch-up compared to that during pitch-down was observed. A similar reduction in u_c (compared to the trend observed in $v_{\theta\text{peak}}$) to values below those of a baseline wing during pitch-up was also observed for the spoiler case (Fig. 7b). No significant variation in u_c was observed during pitch-down, compared to a baseline wing, except for the small reduction in the local peak value of u_c at $\alpha_d = 19$; a local peak of $1.17u_\infty$ compared to $1.3u_\infty$ was noticed. It is significant to note that, in contrast to the marked reduction in Γ and $v_{\theta\text{peak}}$ (as a result of the addition of a spoiler), no noticeable variation in r_c (Fig. 7c), compared to that for a baseline wing, except for the lower$-\alpha$ range during both pitch-up and pitch-down, was observed. The observed increase in r_c in the lower$-\alpha$ range suggests that the effect of a spoiler was most pronounced for the pitch-up attached-flow regime (i.e., before the drastic thickening of the turbulent boundary layer and the onset of flow reversal) and the pitch-down flow-reattachment process. Similar variation in r_o, compared to r_c, was also observed (Fig. 7d), except for large decrease in the outer radius during pitch-up, compared to that for a baseline wing.

The variation of the vortex trajectory under the influence of short-span trailing-edge flaps is summarized in Figs. 7e and 7f. For the spoiler case, the vortex center was found to be shifted further inboard and more vertically upward above the wing, compared to a baseline wing. The vertical displacement of the vortex center during pitch-up was particularly pronounced. Figures 5–7 reveal that for a spoiler-equipped oscillating wing, the tip vortex was altered with its peak tangential velocity and core circulation greatly reduced, and the core vorticity was found to be relatively more diffused or spread out for $\alpha \le \alpha_{ss}$, compared to that for an oscillating baseline wing. The observed favorable substantial reduction in $v_{\theta\text{peak}}$ and Γ_c and basically unchanged r_c (except in the lower$-\alpha$ range), together with the large vertical upward shifting of the vortex trajectory (which translates into an increased miss distance between the tip vortex and the interaction rotor blade at BVI) and the mitigation of undesirable hysteresis in Γ, should certainly lead to a less detrimental effect on the loads during blade–vortex interaction.

The observed reduction in the vortex strength, compared to that for a baseline wing, also suggests an inboard shift of the spanwise circulation $\Gamma(z)$, or lift, distribution. Typical normalized $\Gamma(z)$ distributions, covering $-0.1 \le z/b \le 0.75$, along the wing span with and without passive trailing-edge flaps were determined and are presented in Fig. 8 at selected α. The $\Gamma(z)$ distribution clearly indicates that 1) the lift distribution across a wing varies from a maximum at midspan, or root, to zero at the tips; 2) there was a dip in the $\Gamma(z)$ distribution near the tip for all cases tested, which suggests a tip vortex of greater strength compared to an elliptically loaded wing; and 3) the presence of a small spoiler shifted the tip vortex further inboard with increasing α (Figs. 8a and 8b), compared to a baseline wing, implying a decrease of the tangential velocity. A reduction in the extrapolated bound or root circulation Γ_b at $z = b$ was observed for a spoiler-equipped wing (Fig. 9a), compared to a baseline wing; that is, less lift force was generated in the spoiler-equipped wing-tip region, which gave rise to a lower vortex strength and lift-induced drag, compared to those for a baseline wing. Note that the present

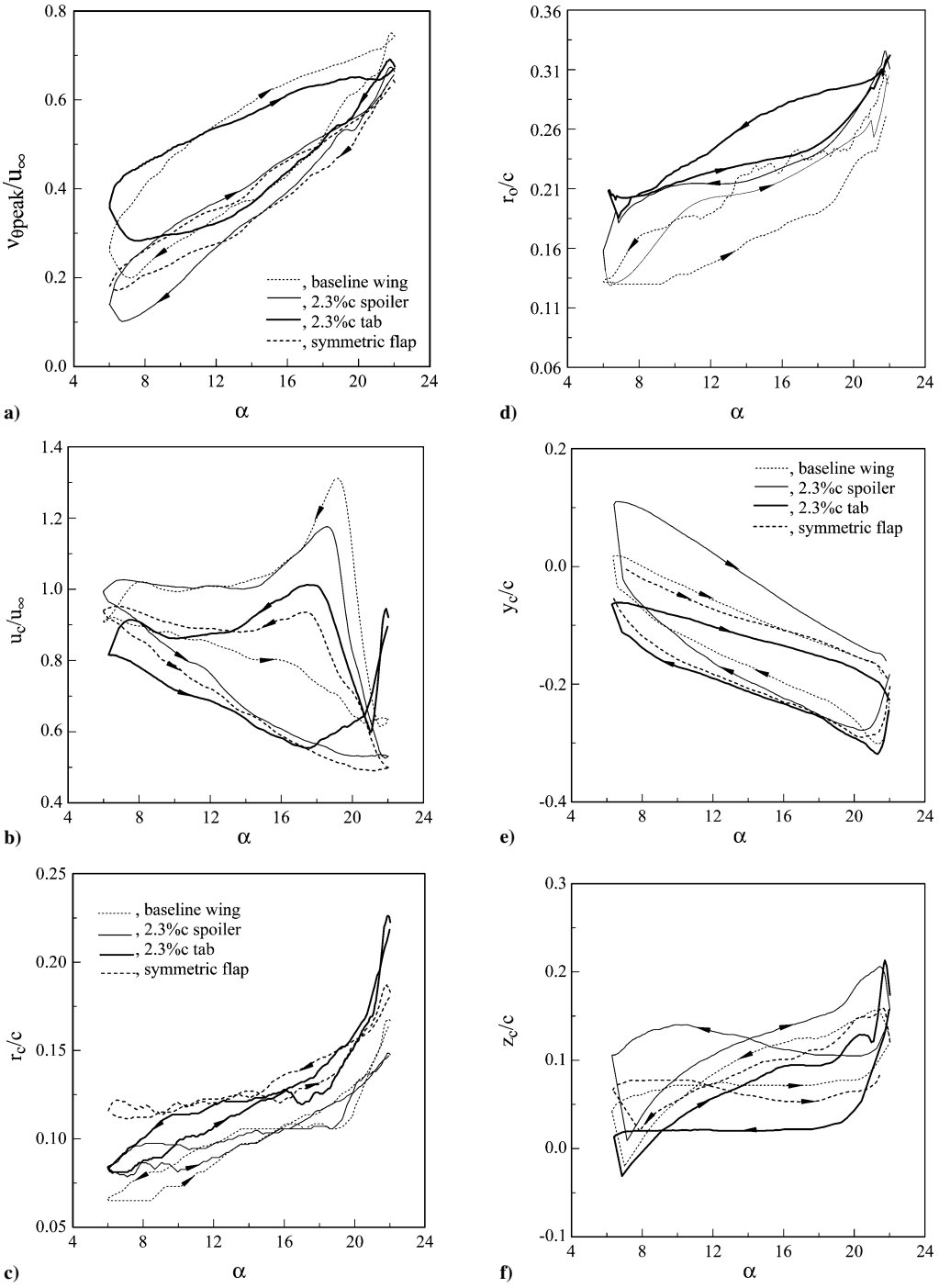

Fig. 7 Dynamic loops of critical vortex flow quantities.

wake flowfield measurements also allow the estimation of the total lift coefficient C_L with the total lift force L obtained from the integration of $\Gamma(z)$ along the wing span through the lifting-line theory,

$$L = \rho U_\infty \int_0^{b/2} \Gamma(z)\,\mathrm{d}z \tag{1}$$

Figure 9b shows that the addition of a spoiler [of height 2.3%c and a span 13%b] caused a slight reduction in C_L during pitch-up, compared to a baseline wing; a much less noticeable reduction was, however, found to exist during pitch-down. The overall behavior of C_L over one oscillation cycle was in good agreement with those of Γ (Fig. 5) and Γ_b (Fig. 9a). There is close similarity and consistency between the curves of Γ_b and C_L. Finally, the lift-induced drag coefficient C_{Di} and the lift-induced drag D_i can also be estimated based on the $\Gamma(z)$ distribution,

$$D_i = L\sin\alpha_i = L\sin\alpha_i(z_0) = \frac{1}{4\pi U_\infty}\int_{-b/2}^{b/2}\left[\frac{(\mathrm{d}\Gamma/\mathrm{d}z)\,\mathrm{d}z}{z - z_0}\right]\cdot L \tag{2}$$

where α_i is the induced angle. Figure 9c clearly indicates that the spoiler-induced reduction in the vortex strength and lift also translates into a similar reduction in the lift-induced drag coefficient, compared to that of a baseline wing, throughout the entire oscillation cycle.

C. Wing with a Tab or a Symmetric Flap Configuration

The effects of a 2.3%c tab on the tip vortex flow were also examined and are discussed in Figs. 4–9. As expected, the tab-induced

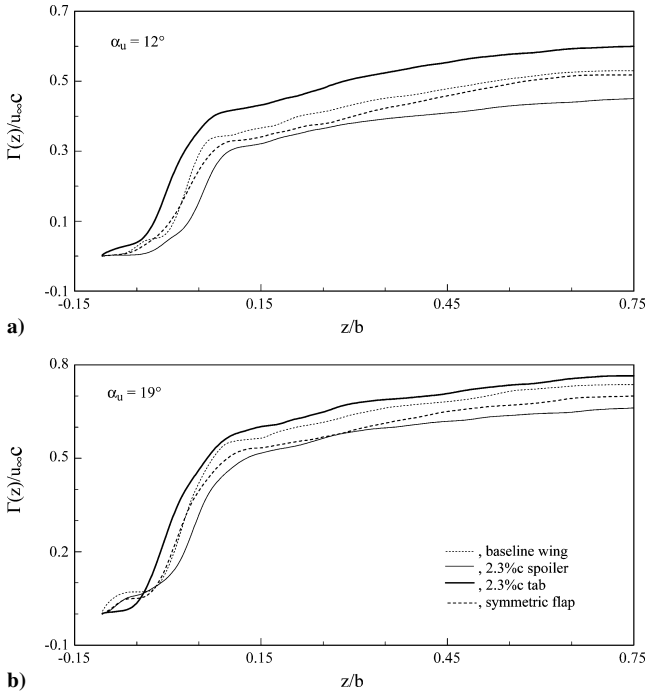

Fig. 8 Typical spanwise circulation distribution.

positive camber effects led to a local increase in the pressure on the lower surface but a decrease on the upper surface (similar to that of a Gurney flap[14]), and, consequently, a vertical upward shift of the lift curve and the dynamic Γ_o and Γ_c curves (in contrast to the downward shift induced by a spoiler), compared to a baseline wing (Fig. 5). The tab, however, only led to a slight change in the degree of asymmetry, or hysteresis, in the dynamic-Γ loops (Fig. 5), compared to a baseline wing. The tip vortex was, however, of much higher ζ contour levels (Fig. 4c), compared to both a baseline wing and the spoiler case, during pitch-up. Also, in contrast to a spoiler, the observed substantial increase in the vortex strength (as shown in Fig. 5) was accompanied by an increased vortex size (Figs. 7c and 7d), compared to a baseline wing. The addition of a tab also led to minor variation in $v_{\theta\text{peak}}$ (compared to a baseline wing; Fig. 7a), in contrast to the substantial reduction for the spoiler case. The u_c curve was found to be shifted vertically downward and was mostly wakelike (Fig. 7b), and had larger velocity deficits during pitch-up than during pitch-down, similar to those of a wing with and without a spoiler. Furthermore, despite the change in location of the centers of concentration of vorticity, the general form of the vortex-flow distributions remained virtually unchanged (Fig. 6); the vortex center was found to move slightly outboard from the wing tip and relatively downward below the wing relative to the trailing edge, compared to a baseline wing, as α was increased and decreased over the entire oscillation cycle (Figs. 7e and 7f). The increase in vortex strength and size and the virtually unchanged $v_{\theta\text{peak}}$, compared to those for a baseline wing, are also reflected by the increase in the $\Gamma(z)$ distribution (Fig. 8) and, consequently, in Γ_b and C_L as well (Figs. 9a and 9b). Note that the dip in the near-tip $\Gamma(z)$ distribution, as shown in Fig. 8, was found to be shifted further outboard. Also, in contrast to the reduction in C_{Di} of the spoiler case, the addition of a tab led to an increase in C_{Di}, compared to that of a baseline wing. In other words, the tab delayed the trailing-edge flow separation and the dynamic lift stalling and rendered an increase in Γ_b and C_L, compared to a baseline wing, but at the price of increased C_{Di}.

Finally, the possibility of the passive control of both the detrimental hysteresis in the dynamic circulation loops and the desirable increase in r_c and decrease in $v_{\theta\text{peak}}$ of an oscillating airfoil via short-span tabs or spoilers can also be reflected in the application of a symmetric flap configuration (Fig. 1b). The results show that the 2.3%c/2.3%c configuration provided a compromise, in terms of the

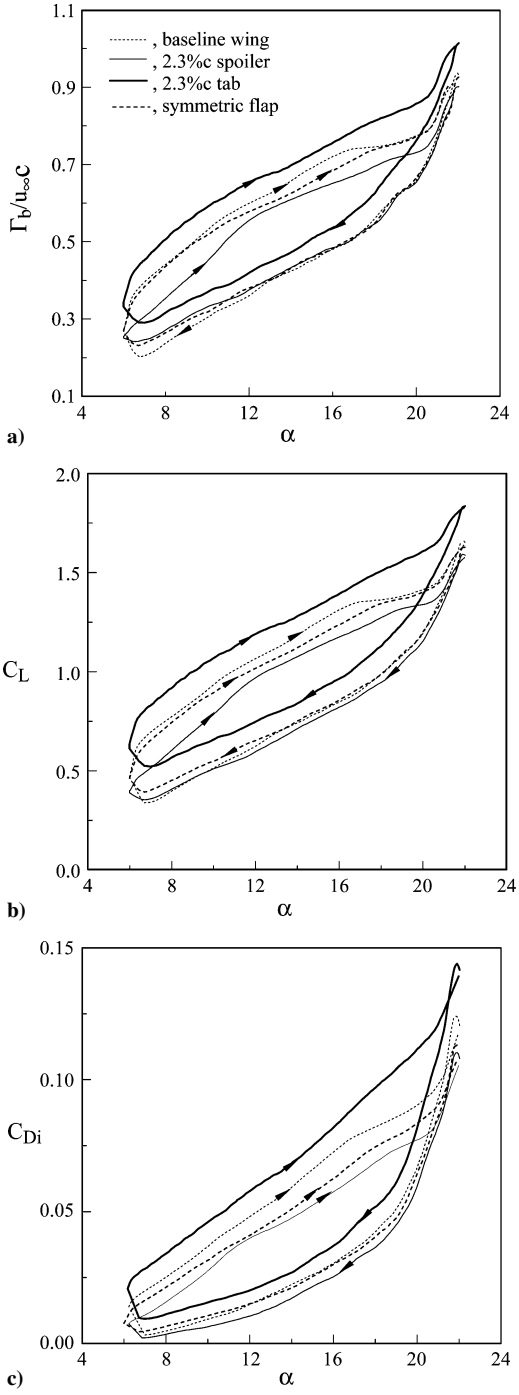

Fig. 9 Γ_b and coefficients of C_L and C_{Di}.

reduction of $v_{\theta\text{peak}}$ and Γ_c and the increase in r_c and the displacement of the vortex trajectory between a (2.3%)c spoiler and a 2.3% tab. The influence of a symmetric flap on the critical vortex flow quantities is summarized in Figs. 5–9 (denoted by dashed lines) and Fig. 4d. In summary, the addition of passive tabs and/or spoilers to an oscillating wing should provide another look into the control of rotorcraft and also the blade–vortex interaction (BVI) via an actively controlled trailing-edge tab, which involves a combination of upward and downward tab deflections of selected tab actuation duration and amplitude and start time.

IV. Conclusions

The tip vortex behind a sinusoidally oscillating NACA 0015 wing with and without short-span trailing-edge flaps was investigated at $\kappa = 0.093$ and $x/c = 2$ and $Re = 1.81 \times 10^5$. The small trailing-edge flaps imposed a strong discrepancy in the vorticity contour

shapes and the magnitudes of the critical vortex flow quantities between the pitch-up and pitch-down phases of the oscillation cycle, compared to a baseline wing. The spoiler was found to be very effective in diffusing the tip vortex. Because much of the lift generated at the tip was destroyed, the tip vortex was subsequently weaker than that of a baseline wing. The addition of a spoiler also resulted in an additional vertical upward displacement of the vortex center (i.e., an equivalent favorable increase in the miss distance at BVI) and a reduced $v_{\theta\text{peak}}$, compared to that of a baseline wing, implying lower induced velocities at BVI. However, no significant change in the vortex size was observed. Also, similarly to a baseline wing, the vortex strength and $v_{\theta\text{peak}}$ were found to be higher during pitch-up than during pitch-down, whereas an opposite trend was exhibited in variation of vortex size and axial core velocity. The spoiler-induced negative camber effects also translated to a slightly reduced Γ_b, C_L, and C_{Di}. For a tab, the dynamic increase–decrease in the vortex size and strength (with no significant change in $v_{\theta\text{peak}}$ comparing to a baseline wing) persisted, while the corresponding magnitudes were above the baseline-wing values, as a result of the tab-induced positive camber effects. The axial core velocity was always wakelike, and the vortex center was shifted relatively outboard and vertically downward below the wing, compared to baseline wing. The tab also led to an increase in C_L and C_{Di}. The symmetric flap provided a compromise in the tip vortex strength, size, and trajectory between the spoiler and tab cases. Detailed knowledge of the wing loadings, especially in the trailing-edge region, however, is needed to better quantify the findings reported here.

Acknowledgment

This work was supported by the Natural Science and Engineering Research Council (NSERC) of Canada.

References

[1]McCroskey, W. J., "Unsteady Airfoils," *Annual Review of Fluid Mechanics*, Vol. 14, 1982, pp. 285–311.

[2]Freymuth, P., Finaish, F., and Bank, W., "Visualization of Wing-Tip Vortices in Accelerating and Steady Flow," *Journal of Aircraft*, Vol. 23, No. 9, 1985, pp. 730–733.

[3]Ramaprian, B. R., and Zheng, Y., "Near Field of the Tip Vortex Behind an Oscillating Rectangular Wing," *AIAA Journal*, Vol. 36, No. 7, 1998, pp. 1263–1269.

[4]Chang, J. W., and Park, S. O., "Measurement in the Tip Vortex Roll-up Region of an Oscillating Wing," *AIAA Journal*, Vol. 38, No. 6, 2000, pp. 1092–1095.

[5]Lee, T., and Gerontakos, P., "Investigation of Flow over an Oscillating Airfoil," *Journal of Fluid Mechanics*, Vol. 512, 2004, pp. 313–341.

[6]Tangler, J. L., "Experimental Investigation of the Subwing Tip and Its Vortex Structure," NASA CR-3058, 1978.

[7]Liu, Z., Russell, W., Sankar, L. N., and Hassan, A. A., "A Study of Rotor Tip Vortex Structure Alternation Techniques," *Journal of Aircraft*, Vol. 38, No. 3, 2001, pp. 473–477.

[8]Muller, R. H. G., "Winglets on Rotor Blades in Forward Flight—A Theoretical and Experimental Investigation," *Vertica*, Vol. 14, No. 1, 1990, pp. 31–46.

[9]Lee, S., "Reduction of Blade–Vortex Interaction Noise through Porous Leading Edge," *AIAA Journal*, Vol. 32, No. 3, 1994, pp. 480–488.

[10]Hardin, J. C., and Lamkin, S. L., "Concepts for Reduction of Blade/Vortex Interaction Noise," *Journal of Aircraft*, Vol. 24, No. 2, 1987, pp. 120–125.

[11]Nguyen, K., "Active Control of Helicopter Blade Stall," *Journal of Aircraft*, Vol. 35, No. 1, 1998, pp. 91–98.

[12]Brooks, T. F., Booth, E. R., Boyd, D. D., Niesl, G. H., and Streby, O., "Analysis of a Higher Harmonic Control Test to Reduce Blade Vortex Interaction Noise," *Journal of Aircraft*, Vol. 31, No. 6, 1994, pp. 1341–1349.

[13]Feszty, D., Cillies, E. A., and Vezza, M., "Alleviation of Airfoil Dynamic Stall Moments via Trailing-Edge-Flap Flow Control," *AIAA Journal*, Vol. 42, No. 1, 2004, pp. 17–25.

[14]Gerontakos, P., and Lee, T., "Oscillating-Wing Loadings with Trailing-Edge Strips," *Journal of Aircraft* (to be Published).

[15]Wenger, C. W., and Devenport, W. J., "Seven-Hole Pressure Probe Calibration Utilizing Look-Up Error Tables," *AIAA Journal*, Vol. 37, No. 6, 1999, pp. 675–679.

[16]Chow, J. S., Zilliac, G. G., and Bradshaw, P., "Mean and Turbulence Measurements in the Near Field of a Wingtip Vortex," *AIAA Journal*, Vol. 35, No. 10, 1997, pp. 1561–1567.

[17]Birch, D., and Lee, T., "Structure and Induced Drag of a Tip Vortex," *Journal of Aircraft*, Vol. 41, No. 5, 2004, pp. 1138–1145.

[18]Ericsson, L. E., and Reding, J. P., "Fluid Mechanics of Dynamic Stall. Part I. Unsteady Flow Concepts," *Journal of Fluids and Structures*, Vol. 2, No. 1, 1988, pp. 1–33.